ORIGINAL ARTICLE

A Fibrocontractive Mechanochemical Model of Dermal Wound Closure Incorporating Realistic Growth Factor Kinetics

**Kelly E. Murphy · Cameron L. Hall ·
Philip K. Maini · Scott W. McCue ·
D.L. Sean McElwain**

Abstract Fibroblasts and their activated phenotype, myofibroblasts, are the primary cell types involved in the contraction associated with dermal wound healing. Recent experimental evidence indicates that the transformation from fibroblasts to myofibroblasts involves two distinct processes: The cells are stimulated to change phenotype by the combined actions of transforming growth factor β (TGFβ) and mechanical tension. This observation indicates a need for a detailed exploration of the effect of the strong interactions between the mechanical changes and growth factors in dermal wound healing. We review the experimental findings in detail and develop a model of dermal wound healing that incorporates these phenomena. Our model includes the interactions between TGFβ and collagenase, providing a more biologically realistic form for the growth factor kinetics than those included in previous mechanochemical

K.E. Murphy (✉) · S.W. McCue · D.L.S. McElwain
School of Mathematical Sciences, Queensland University of Technology, Brisbane, QLD 4001, Australia
e-mail: kelly.murphy@qut.edu.au

K.E. Murphy · D.L.S. McElwain
Tissue Repair and Regeneration Program, Institute of Health and Biomedical Innovation, Queensland University of Technology, Brisbane, QLD 4001, Australia

C.L. Hall
Oxford Centre for Collaborative Applied Mathematics, Mathematical Institute, University of Oxford, 24-29 St Giles', Oxford, OX1 3LB, UK

P.K. Maini
Centre for Mathematical Biology, Mathematical Institute, University of Oxford, 24-29 St Giles', Oxford OX1 3LB, UK

P.K. Maini
Oxford Centre for Integrative Systems Biology, Department of Biochemistry, University of Oxford, South Parks Road, Oxford, OX1 3QU, UK

descriptions. A comparison is made between the model predictions and experimental data on human dermal wound healing and all the essential features are well matched.

Keywords Biomechanics · Myofibroblasts · Transforming growth factor-β · Contraction

1 Introduction

The process of dermal repair is intricate and the resulting scar is inferior to unwounded tissue in several aspects. Aberrant healing may result in pathological scarring that can cause both physical and psychosocial distress to the patient (Herber et al. 2007; Brown et al. 2008, 2010). Understanding and elucidating the mechanisms that elicit normal and regenerative repair is vital to ameliorating the wound healing response.

There are various ways of characterizing the stages of acute healing. A recent description proposed by Enoch et al. (2006) separates wound healing into four overlapping, yet distinct, phases. The first two are: (1) haemostasis, which involves arresting blood flow through the establishment of a fibrin clot (Monroe et al. 2010) and (2) inflammation, where neutrophils, macrophages, and other leukocytes debride the wound, removing necrotic cells, and damaged tissue (Enoch and Leaper 2007). These cells also release growth factors that attract fibroblasts, the main cell type in dermal repair, to the wound (Shultz et al. 2005). The other stages are: (3) proliferation and (4) epithelialisation and remodelling. As the model we describe concerns these final two phases, we now discuss these stages in more detail.

The proliferative phase begins around day 4 post-wounding when fibroblasts are recruited from the surrounding undamaged tissue (Shultz et al. 2005). These cells proliferate and are activated to become myofibroblasts. Both fibroblasts and myofibroblasts function as the primary contractile cells in wound repair, with myofibroblasts exerting stronger cell traction stresses than fibroblasts (Wipff and Hinz 2009). Together, these cells synthesize proteins such as collagen to replace the fibrin network, and they remodel the resulting collagen lattice (Hinz 2007). Concurrently, endothelial cells migrate into the wound space, revascularising the wound in a process known as angiogenesis (Enoch and Leaper 2007). The proliferating fibroblasts, loose collagen network and neovascularised tissue form a temporary contractile organ known as granulation tissue (Enoch and Leaper 2007). The contraction of granulation tissue due to the action of fibroblasts and myofibroblasts results in a wound reduction of up to 30% in humans (Desmouliere et al. 1995; Hinz et al. 2001; Farahani and Kloth 2008) and up to 80% in rats (Farahani and Kloth 2008). Finally, the onset of reepithelialisation signals the final phase of proliferation.

In the fourth and final stage of wound healing, the outer epidermal layer is restored. Fibroblasts continue to remodel the extracellular matrix, increasing the tensile strength of the wound from approximately 20% to 70% of normal dermal strength after several months of remodelling (Cotran et al. 1999; Singer and Clark 1999). Finally, a mature scar consisting mainly of collagen develops.

The mathematical literature abounds with investigations into wound repair. Just a sample of the diverse topics considered include angiogenesis (Pettet et al. 1996;

Tranqui and Tracqui 2000; Schugart et al. 2008), the interaction between fibroblast and collagen fibre orientation (Dallon and Sherratt 1998; Dallon et al. 1999, 2001; McDougall et al. 2006; Cumming et al. 2010), effects due to growth factors (Dale et al. 1997; Vermolen and Javierre 2010), simple mechanical effects (Tranquillo and Murray 1992; Tracqui et al. 1995; Murray et al. 1997; Murray 2003), myofibroblast-enhanced contraction (Olsen et al. 1995, 1996), the interaction between the collagen lattice and extracellular fluid during contraction (Barocas and Tranquillo 1997), the effects of matrix anisotropy (Cook 1995), abnormal dermal repair (Waugh and Sherratt 2006; Thackham et al. 2008; Xue et al. 2009; Flegg et al. 2010) and models incorporating a combination of wound healing phenomena (Javierre et al. 2009; Hall 2009; Murphy et al. 2011). However, none of these studies include an explicit description of the mechanical interaction between the cells and their viscoelastic substrate of extracellular matrix (ECM) coupled with a realistic description of the chemical kinetics. We address this issue in the current article.

The first mechanochemical models for dermal wound healing were developed by Murray et al. (1988) and Tranquillo and Murray (1992). The key feature of these models is the mechanical interaction between the cells and their viscoelastic substrate of extracellular matrix (ECM). The "base" Tranquillo–Murray model comprises three governing equations; two of these stipulate the rate of change of the fibroblast concentration, n, and the ECM density, ρ, respectively, while the third describes a force balance, from which the velocity of the ECM is derived. In one-dimensional Cartesian coordinates, the base non-dimensional model takes the following form:

$$\text{Cells:} \quad \frac{\partial n}{\partial t} + \frac{\partial}{\partial x}\left(n\frac{\partial u}{\partial t}\right) = \frac{\partial^2 n}{\partial x^2} + rn(1-n); \tag{1}$$

$$\text{ECM:} \quad \frac{\partial \rho}{\partial t} + \frac{\partial}{\partial x}\left(\rho\frac{\partial u}{\partial t}\right) = 0; \tag{2}$$

$$\text{Force Balance:} \quad s\rho u = \frac{\partial}{\partial x}\left(\sigma + \mu\frac{\partial v}{\partial x} + \psi\right); \tag{3}$$

$$\text{Elastic Force:} \quad \sigma = \frac{\partial u}{\partial x}; \tag{4}$$

$$\text{Cell-Traction Force:} \quad \psi = \frac{\tau\rho n}{1+\gamma n^2}; \tag{5}$$

$$\text{Velocity:} \quad v = \frac{\partial u}{\partial t}; \tag{6}$$

where x is the distance from the wound centre, u is the ECM displacement, μ is the viscosity of the tissue, γ is a parameter quantifying "social loafing" (the amount that a species will stop doing work in the presence of other members of the same species), s is the tethering coefficient of the dermal layer to the subcutaneous tissue, τ is a measure of the fibroblast traction on ECM fibres, and r is the intrinsic growth rate of fibroblasts. The model considers a symmetric wound about $x = 0$, with the wound located on $0 < x < L$, such that $2L$ is the width of the wound. The region $x > L$ corresponds to the surrounding unwounded dermis.

While this seminal model laid the groundwork for much of the subsequent years of research in this area, it neglected some of the essential features of wound healing, such as collagen biosynthesis and heightened collagen density in the wound space. Moreover, this model is unable to describe the significant wound boundary contraction common in dermal repair. While Tranquillo and Murray (1992) did extend their model to incorporate some of these features, the limitations of this formulation, together with the wealth of new experimental data means that a more detailed representation has become a necessity.

One of the key simplifying assumptions made by Tranquillo and Murray (1992) was that alterations to the ECM do not modify the mechanical properties of the tissue. However, experimental results reveal that this is not the case (Shultz et al. 2005). In the present study, we aim to improve on this model by assuming, like authors such as Ramtani et al. (2002), that tissue elasticity is dependent upon the collagen density.

Olsen and co-workers extended the work of Tranquillo–Murray in a series of papers (Olsen et al. 1995, 1996, 1997, 1998, 1999). Their first advance considered two distinct cellular populations: fibroblasts and myofibroblasts. Inter-conversion between the two phenotypes is assumed, and this is taken to be dependent on the presence of a growth factor (PDGF). Previously, Tranquillo and Murray (1992), in an extension of (1)–(6), assumed a static distribution for the chemical species. To make the description more realistic, Olsen et al. (1995) incorporated a time-dependent representation. Additionally, Olsen and colleagues included collagen synthesis and degradation. Olsen et al. (1995) was able to predict plastic deformation (permanent wound contraction), but only in the absence of collagen kinetics. However, it is now known that matrix turnover is initially rapid, implying that collagen kinetics should not be neglected. Hence, further modelling is required to generate plastic deformation.

The description developed by Tranquillo and Murray (1992) used a purely viscoelastic formulation for the mechanics. Consequently, the system returns to its original state unless a nonhomogeneous spatial distribution of chemical mediator is assumed. With this in mind, Cook (1995) extended Tranquillo and Murray's work by developing a more realistic representation of tissue mechanics that accounts for the structure of a changing, anisotropic ECM. In so doing, Cook was the first to address tissue growth and remodelling and their associated effects upon tissue mechanics. These effects are also considered in Murphy et al. (2011), who also incorporated direct stress coupling between the cells and their mechanical environment.

When cultured under mechanical strain and/or on a stiff substrate, fibroblasts develop actin stress fibres (Grinnell 2000; Tomasek et al. 2002; Grinnell 2003; Desmouliere et al. 2005). In this state, the cells are termed proto-myofibroblasts, and they exert more cell traction on the ECM than fibroblasts and exhibit upregulated collagen synthesis. Under the action of TGFβ, proto-myofibroblasts differentiate into myofibroblasts, which are distinguished by the presence of α-smooth muscle actin (α-SMA) (Hinz 2007; Wells and Discher 2008; Wipff and Hinz 2008, 2009; Hinz 2010). To our knowledge, Javierre et al. (2009) and Murphy et al. (2011) are the only papers to present mathematical models for dermal wound healing that incorporate the stress-dependency of fibroblast to myofibroblast differentiation. However, neither representation considers the proto-myofibroblast stage, instead adopting a combined proto-myofibroblast and myofibroblast population.

The model developed by Javierre et al. (2009) is an extension of the Olsen et al. (1995) model in which PDGF is assumed to be the chemical involved in activating fibroblasts. While PDGF can induce the formation of proto-myofibroblasts, it does not induce transformation to myofibroblasts or expression of α-SMA (Tomasek et al. 2002). Moreover, Javierre et al. (2009) assume that cell traction stress activates fibroblasts, but Hall (2009) found that, for consistency between the mathematical representation and experimental results, the stress component involved in fibroblast activation is the elastic stress and not the cell traction stress. If fibroblast differentiation is assumed to depend on cell traction stress then the greatest activation occurs outside the lesion, i.e. in the unwounded tissue. This is not physiological, as the myofibroblast presence is greatest within the wound space. In contrast, making differentiation depend on the elastic stress would lead to higher rates of conversion within the wound space itself. Moreover, the cell traction stress can be thought of as a convenient representation of what is actually a body force acting on the tissue. By pulling on the tissue, each cell acts as a force dipole; the net effect of these dipoles is a body force determined by the gradient of the cell traction stress. Thus, the elastic stress is the real stress in the ECM, and it is most reasonable to expect that this is the stress that cells will feel and to which they will respond.

Incorporating these observations into a model means that it is impossible to decouple the mechanics from the biology because there is two-way feedback between cellular behaviour and mechanical stress. In the Olsen et al. (1995) and Tranquillo and Murray (1992) descriptions, passive ECM-mediated advection was the only interaction between the cell and ECM behaviour and the wound mechanics. However, since the velocity was generally small, advection could be neglected without significantly altering the model predictions (Hall 2009). Consequently, the cellular and ECM components could essentially evolve independent of the mechanics. We argue that this coupling is important in light of recent experimental results and so attempt to resolve this issue by incorporating the stress-dependence in the activation of fibroblasts and myofibroblast proliferation.

The model of Murphy et al. (2011) incorporated some of this feedback between the cells and tissue mechanics. This representation extended the work of Olsen et al. (1995), Cook (1995), and Hall (2009), employing a morphoelastic approach to representing the mechanical behaviour instead of the traditional linear viscoelasticity. This model is more appropriate for the large deformations observed in wound repair, but it neglected to develop a detailed approximation to the chemical kinetics and their associated interactions with cellular and extracellular aspects of repair.

The wound healing model proposed by Dale et al. (1997) does not incorporate tissue mechanics, but it contains the most detailed description of the chemical kinetics of the bioactive species in a dermal wound. Here, we adopt a reduced version of the Dale et al. (1997) model, in spite of the fact that this represents a simplification of the *in-vivo* kinetics. Additionally, we modify the model to incorporate recent experimental results.

When comparing model predictions against experimental data, researchers developing mechanochemical representations of dermal repair typically consider the wound contraction dynamics recorded by McGrath and Simon (1983). However, the wound contraction data obtained by McGrath and Simon (1983) are for rat dermal

repair, and mechanochemical modellers are generally seeking to justify a model for human dermal wound healing. Rat and human dermal wounds heal primarily by different mechanisms. While rat wounds heal mainly by contraction, human dermal wounds (while still experiencing contraction) heal primarily as a result of infilling. Thus, we qualitatively compare our predictions against the observations of McGrath and Simon (1983), but seek to ascertain the relevance of our model by comparing our predictions against the wound contraction data obtained by Catty (1965) for human dermal repair.

The role of TGFβ is now considered to be critical to dermal repair but there are, as yet, no mechanochemical models that consider TGFβ as the primary growth factor in dermal repair. Additionally, none include the regulatory effects of collagenase on the collagen density. Here, we incorporate TGFβ and collagenase into a simplified representation of chemical kinetics and then couple this with a description of tissue mechanics and cellular dynamics. With regard to cellular interactions, our model includes a novel representation of the fibroblast to myofibroblast activation.

We develop our proposed model in Sect. 2 below and present the model results in Sect. 3. Our model predicts early retraction followed by contraction and late retraction. The results are compared with two sets of experimental data on wound closure, that of Catty (1965) for human wounds, and that of McGrath and Simon (1983) for rat dermal repair. We seek only to obtain qualitative agreement with the McGrath and Simon data. Our analysis shows that the model predicts all phases of wound repair (retraction, contraction, permanent contraction, and late retraction) for both situations.

2 Mathematical Model

We consider seven dependent variables in our model: fibroblast density (n), myofibroblast density (m), transforming growth factor-β concentration (β), platelet-derived growth factor concentration (P), collagen density (ρ), collagenase density (z), ECM displacement (u) and velocity (v). We assume that the wound is long and thin, and that it is much longer than it is deep. As such, a one-dimensional representation is appropriate.

We assume that a small strain representation is valid and thus the velocity can be approximated by the Eulerian time derivative of displacement:

$$v = \frac{\partial u}{\partial t}. \tag{7}$$

2.1 Force Balance Equation

Following Tranquillo and Murray (1992), we neglect inertial forces and so the momentum conservation equation reduces to a mechanical force balance between the forces related to the physico-chemical ECM properties (consisting of tethering to the underlying fascia, elastic, and viscous forces) and the cell-generated traction forces.

We assume that the tethering force is proportional to the local collagen concentration and tissue displacement. Together, this gives the following force balance equation:

$$s\rho u = \frac{\partial}{\partial x}\left(\sigma + \mu\frac{\partial v}{\partial x} + \psi\right),\tag{8}$$

where s is the tethering coefficient, μ is the tissue viscosity, and σ and ψ represent the elastic and cell traction forces, respectively.

Since we are considering a linear viscoelastic framework, the elastic force is proportional to the deformation gradient (Skalak et al. 1996). However, we further assume that variations in collagen density will affect the elastic modulus (Ramtani et al. 2002; Ramtani 2004). Specifically, we will assume that the elastic modulus is directly proportional to the collagen density, with a constant of proportionality, E. Thus, σ takes the form

$$\sigma = E\rho\frac{\partial u}{\partial x}.\tag{9}$$

There are a number of possible expressions for cell traction. Following Tranquillo and Murray (1992), we assume that cell traction forces depend upon the product of the cellular and collagen densities. We also assume that fibroblasts and myofibroblasts contribute differently to cell traction but we do not include any 'social loafing' terms. This gives

$$\psi = \lambda\rho(n + \xi m),\tag{10}$$

where λ is a constant and ξ is the myofibroblast tractional stress relative to fibroblast tractional stress. We note that Olsen et al. (1995) assume that myofibroblasts increase the cell traction generated by the fibroblasts, but that myofibroblasts do not work independently to enhance cell traction. However, Tomasek et al. (2002) indicates that myofibroblasts work independently of fibroblasts to effect contraction. Also, we note that other expressions for cell traction could be adopted in which ψ is no longer directly proportional to n, m, or ρ (see Tranquillo and Murray 1992, and Olsen et al. 1995). It is preferable to use the simplest form available for cell traction consistent with experimental observations, and so we adopt the above expression.

2.2 Fibroblasts

We assume that the fibroblasts exhibit random motility (modelled by diffusion), PDGF-mediated chemotaxis and experience ECM-mediated advection. TGFβ stimulates fibroblast proliferation which, in the absence of other factors, is assumed to be logistic. Fibroblast to myofibroblast transformation requires tension (represented by positive elastic stress) and the presence of active TGFβ. Hence, we obtain

$$\frac{\partial n}{\partial t} + \frac{\partial}{\partial x}(nv) = \frac{\partial}{\partial x}\left[D_n\frac{\partial n}{\partial x} - \frac{\chi n}{(a_\chi + P)^2}\frac{\partial P}{\partial x}\right]$$
$$+ (1 + a_{n\beta}\beta)n\big(r - \theta_{nn}(n + m)\big) - \alpha\sigma^+\beta n,\tag{11}$$

where D_n is the fibroblast random motility coefficient, χ is the chemotactic coefficient, a_χ represents the half-maximal response, α is the fibroblast differentiation rate,

σ^+ represents the positive elastic stress, $a_{n\beta}$ represents the upregulation of fibroblast proliferation in the presence of TGFβ, r is the intrinsic fibroblast proliferation rate, and θ_{nn} represents the reduction in proliferation due to crowding.

Since there is insufficient experimental evidence to suggest otherwise, we assume that myofibroblasts do not transform back to fibroblasts, but instead undergo apoptosis (Moulin et al. 2004; Hinz 2007; Farahani and Kloth 2008). However, we note that Olsen et al. (1995) include the reversion of myofibroblasts to fibroblasts. Moreover, we do not include a proto-myofibroblast population, and instead consider a combined proto-myofibroblast and myofibroblast population, which we simply refer to as myofibroblasts.

2.3 Myofibroblasts

Without evidence that myofibroblasts are actively motile, we assume that their transport is due only to ECM-mediated advection. As long as the granulation tissue is under stress, myofibroblasts will proliferate (Grinnell 1994; Hinz 2007). Hence, we follow Hall (2009) and assume that myofibroblasts only proliferate under stress and that this growth is bounded. Finally, myofibroblasts undergo natural cell death. Together, these assumptions give

$$\frac{\partial m}{\partial t} + \frac{\partial}{\partial x}(mv) = m\big(a_{m\sigma}\sigma^+(1 + a_{m\beta}\beta) - \theta_m - \theta_{mm}(n + m)\big) + \alpha\sigma^+\beta n, \quad (12)$$

where $a_{m\beta}$ represents the upregulation in myofibroblast proliferation under the action of TGFβ, $a_{m\sigma}$ is the intrinsic myofibroblast proliferation rate under tension, θ_m is the natural cell death rate and θ_{mm} represents the decrease in proliferation due to crowding.

2.4 TGFβ

TGFβ diffuses and is passively advected by the ECM. This growth factor is produced by both fibroblasts and myofibroblasts (Hinz 2007; Wipff et al. 2007), with production inhibited by the presence of TGFβ (Dale et al. 1996). We recognise that TGFβ is synthesized by cells in a latent form, which is then activated by one of two mechanisms. These are the activation by myofibroblasts from large latent complex stores attached to the ECM (Wipff et al. 2007; Wells and Discher 2008) and the cleavage of circulating latent TGFβ by collagenases (Dale et al. 1996). For simplicity, we consider a combined latent and active TGFβ species. TGFβ also undergoes natural decay. Incorporating all of these effects into a model, we obtain:

$$\frac{\partial \beta}{\partial t} + \frac{\partial}{\partial x}(\beta v) = D_\beta \frac{\partial^2 \beta}{\partial x^2} + \frac{a_\beta \beta(n + \pi m)}{1 + b_\beta \beta} + a_{\beta m}m\rho + a_{\beta z}z\beta - \delta_\beta \beta, \quad (13)$$

where D_β is the TGFβ diffusivity, a_β characterizes the production rate of TGFβ by fibroblasts, π is the ratio of myofibroblast to fibroblast production of TGFβ, $a_{\beta m}$ is the activation rate of TGFβ from matrix stores, $a_{\beta z}$ is the activation rate of latent TGFβ by collagenases and δ_β is the decay rate of TGFβ. We adopt a saturation form for the production of TGFβ, with b_β related to the half-maximal rate of production.

2.5 PDGF

Macrophages and other cells produce PDGF, which we assume occurs at a constant rate, a_P. PDGF also experiences natural decay and depletion through endocytosis by both fibroblasts and myofibroblasts, with myofibroblasts assumed to uptake the same amount of PDGF as fibroblasts. Finally, PDGF diffuses and is advected by the ECM. Thus,

$$\frac{\partial P}{\partial t} + \frac{\partial}{\partial x}(Pv) = D_p \frac{\partial^2 P}{\partial x^2} + a_P - \delta_P P - \delta_{Pn}(n+m)P, \qquad (14)$$

where D_P is the PDGF diffusivity, δ_P represents natural decay and δ_{Pn} denotes fibroblast and myofibroblast-mediated PDGF depletion.

2.6 Collagen

Collagen undergoes ECM-mediated advection and is synthesized by both cell types, with production upregulated by the presence of TGFβ. Additionally, collagen is degraded by the action of collagenases. Thus, we obtain

$$\frac{\partial \rho}{\partial t} + \frac{\partial}{\partial x}(\rho v) = k(n + \eta m)(1 + a_{\rho\beta}\beta) - \delta_\rho \rho z, \qquad (15)$$

where k characterizes the production rate of collagen by fibroblasts, η is the ratio of myofibroblast to fibroblast collagen production, $a_{\rho\beta}$ is a measure of the increase in synthesis due to the presence of TGFβ and δ_ρ is the degradation rate. Note that we refer to collagen and ECM interchangeably throughout the rest of this paper, since dermal ECM consists mainly of collagen.

2.7 Collagenase

While several species of collagenase are involved in the wound healing process, we consider here a general representation of these enzymes. Since collagenase binds to the local ECM, we assume that diffusion is negligible and thus collagenase transport is only by ECM-mediated advection (Dale et al. 1997). Both fibroblasts and myofibroblasts secrete collagenase in the presence of collagen, with production of collagenase inhibited by the presence of active TGFβ (Wipff and Hinz 2009). Furthermore, collagenase undergoes natural decay. Putting this together, we have

$$\frac{\partial z}{\partial t} + \frac{\partial}{\partial x}(zv) = \frac{a_z \rho(n + \zeta m)}{1 + b_z \beta} - \delta_z z, \qquad (16)$$

where a_z characterizes the production rate of collagenase by cells in the presence of collagen, ζ is the rate of myofibroblast collagenase synthesis relative to fibroblast collagenase synthesis, b_z measures the inhibition of collagenase synthesis due to the presence of TGFβ, and δ_z is the collagenase decay rate.

We note that collagenase is secreted by cells in a latent form that is activated through proteolytic cleavage. Dale et al. (1997) incorporate this feature into their

model. However, for simplicity, we have chosen to combine the latent and active forms of collagenase as a single species. We also note that collagenases are a subset of the matrix metalloproteinases (MMPs) and that the collagenase in this model could be identified with MMP-1. Both Chakraborti et al. (2003) and Jenkins (2008) provide extensive reviews of MMPs in ECM.

2.8 Initial/Boundary Conditions and Non-dimensionalization

The initial conditions of our model refer to the state of the wound at the onset of the proliferative phase. At this stage, we take the wound to occupy $-L < x < L$, so that L represents the wound boundary. We assume:

1. Symmetry about $x = 0$, and so we can restrict ourselves to considering the domain where x is positive;
2. $x > L$ represents unwounded tissue;
3. The characteristic time scale of the model, T, is one day;
4. There are no fibroblasts within the wound space and they are at unwounded levels outside;
5. The initial myofibroblast density is zero everywhere;
6. Due to growth factor release in the inflammatory stage, TGFβ is present inside the wound space, but not outside;
7. Within the wound, PDGF is initially at its steady state value in the case of no fibroblasts, while outside the lesion PDGF takes its steady state value appropriate for the situation in which fibroblasts are present;
8. There is a small amount of collagen in the wound space initially, while unwounded levels prevail outside; and
9. Collagenase is only produced in the presence of collagen, and thus that there is no collagenase in the wound initially and that it is at unwounded levels outside.

To avoid discontinuities which can give rise to numerical instabilities when solving the PDE system, we approximate these piecewise conditions using tanh functions (see Appendix B for details).

Immediately following injury, there is an almost instantaneous retraction of the wound boundary (see for example Billingham and Medawar 1955; Catty 1965). Indeed, the unwounded dermis surrounding the wound has an elastic tension that tends to draw the wound edges apart (Watts 1960; Kennedy and Cliff 1979). Therefore, the initial displacement is not zero throughout the domain, but is rather found by demanding the force balance expression (8) hold. Since this initial retraction is driven by elastic tension, we neglect viscosity when determining the initial displacement.

The symmetry around $x = 0$ implies zero flux conditions for all species other than displacement and velocity, which must necessarily be zero at the wound centre. For numerical purposes, all species are assumed to take on their unwounded values at the right-hand boundary (far away from the wound site),

$$n(x_{\text{RH}}, t) = n_U, \qquad m(x_{\text{RH}}, t) = 0, \qquad \beta(x_{\text{RH}}, t) = \beta_U, \qquad P(x_{\text{RH}}, t) = P_U,$$

$$\rho(x_{\text{RH}}, t) = \rho_U, \qquad z(x_{\text{RH}}, t) = z_U, \qquad u(x_{\text{RH}}, t) = 0,$$

where x_{RH} is the position of the right hand boundary and $x_{\text{RH}} \gg L$, and n_U, β_U, P_U, ρ_U, and z_U represent the unwounded densities of fibroblasts, TGFβ, collagen and collagenases, respectively.

The system was non-dimensionalized (see Appendix A), discretised using finite difference approximations in space and solved numerically using MATLAB's inbuilt routine, *ode45*. We consider a grid size of 401 and a computational domain of 10 semi-wound lengths; this ensures that the right-hand boundary is far enough from the wound site so as not to affect the solution within the wound. Grid independent results are obtained providing the grid size exceeds 301 nodes. Advective terms are determined by solving the tri-diagonal system obtained by discretising the force balance expression, (8), with displacement found by subsequently using (7).

2.9 Parameter Values

Almost all parameter values have been estimated from experimental results or taken from previous models of dermal repair. Table 1 contains the dimensional values of the parameters together with the source of the data; if a given parameter has been estimated in this work, this is indicated by TW. The sensitivity analysis shows our model to be quite robust to significant variations in a number of parameter values. For a full discussion on parameter estimation, see Appendix C.

3 Results

Figures 1–5 show the results obtained from the numerical solution of the system of governing equations and we now discuss these in detail.

3.1 Fibroblasts

Initially, there are no fibroblasts inside the wound space and they are at unwounded levels outside. While fibroblasts are recruited from the surrounding dermis, proliferation is the primary mode by which the fibroblast population within the wound space is restored. There is significant conversion of fibroblasts to myofibroblasts over the first fortnight of repair, which accounts for the unusual shape of the fibroblast distribution. Indeed, the mechanical stimulation of fibroblast activation impedes the restoration of the fibroblast density within the wound space through modulation to myofibroblasts. Nonetheless, by day 30, the fibroblast density across the domain has essentially been restored to undamaged tissue values. We note that varying the chemotactic coefficient has little impact on the model predictions.

3.2 Myofibroblasts

Initially, there are no myofibroblasts in the system. Fibroblasts are activated to become myofibroblasts under the action of elastic stress and TGFβ, and, for this parameter set, this conversion is found to be the primary source of myofibroblasts. Differentiation of fibroblasts generates a population of myofibroblasts within the wound domain, which proliferate and generate stress. Thus, myofibroblasts contribute to both

Table 1 Table of parameters, which unless otherwise specified, are used for all simulations. TW refers to parameters that were estimated during this work. The determination of all parameter values is discussed in Appendix C

Parameter	Range	Reference
D_n, Fibroblast random motility	$D_n \approx O(10^{-3})$ cm^2/day	Sillman et al. (2003)
χ, Chemotaxis	$\chi \approx 0.03$ ng/cm day	Haugh (2006), TW
a_χ, Half-maximal response	$a_\chi \approx 2$ ng/cm^3	Olsen et al. (1995)
r, Fibroblast proliferation	$0.832 < r < 0.924$/day	Ghosh et al. (2007)
$a_{n\beta}$, Enhancement of fibroblast proliferation by TGFβ	$a_{n\beta} \approx 2/\beta_0$	Strutz et al. (2001)
θ_{nn}, 1/Fibroblast carry capacity	$\theta_{nn} \approx 10^{-6}$ cells	Vande Berg et al. (1989)
α, Fibroblast activation to myofibroblasts	$r \approx 0.0108$/day (ng/mL)	Desmouliere et al. (1993)
$a_{m\sigma}$, Myofibroblast proliferation	$a_{m\sigma} \approx 0.5r$	Vande Berg et al. (1989)
$a_{m\beta}$, Enhancement of myofibroblast proliferation by TGFβ	$a_{m\beta} \approx a_{n\beta}$	Olsen et al. (1995)
θ_m, Myofibroblast apoptosis	$\theta_m \approx 0.9$/day	Olsen et al. (1995)
θ_{mm}, 1/Myofibroblast carrying capacity	$\theta_{mm} \approx 2\theta_{nn}$	Masur et al. (1996)
D_β, TGFβ diffusivity	$D_\beta \approx 0.0254$ cm^2/day	Stokes–Einstein Formula
a_β, TGFβ synthesis by fibroblasts	$a_\beta \approx 0.125 \times 10^{-6}$ ng/cell day	Wang et al. (2000)
π, TGFβ synthesis by myofibroblasts relative to fibroblasts	$\pi \approx 2$	Kim and Friedman (2009)
b_β, Inhibition of TGFβ synthesis	$b_\beta \approx 5/\beta_0$	Dale et al. (1995)
$a_{\beta m}$, TGFβ activation by myofibroblasts	$a_{\beta m} \approx 4.35 \times 10^{-9}$ mL day/cell	Order of magnitude estimate, TW
$a_{\beta z}$, TGFβ activation by proteolytic cleavage	$a_{\beta z} \approx 0.0014$ mL/ng day	Order of magnitude estimate, TW
δ_β, TGFβ decay	$b \approx 0.354$/day	Yang et al. (1999)
D_P, PDGF diffusion coefficient	$D_P \approx 2.88 \times 10^{-3}$ cm^2/day	Haugh (2006)
a_P, PDGF production	$a_P \approx 24$ ng/cm^3 day	Monine and Haugh (2008), TW
δ_P, PDGF degradation	$\delta_P \approx 2.4$/day	Haugh (2006)
δ_{Pn}, fibroblast-mediated PDGF depletion	$\delta_{Pn} \approx 2.4 \times 10^{-5}$/cell day	Haugh (2006), TW Monine and Haugh (2008)
k, Collagen production	$k \approx 1.75$ pg/cell day	Bahar et al. (2004)
η, Relative collagen production by myofibroblasts	$\eta \approx 2$	Moulin et al. (1998), Olsen et al. (1995)
$a_{\rho\beta}$, Enhancing of collagen production by TGFβ	$a_{\rho\beta} \approx 2/\beta_0$	Eickelberg et al. (1999)
δ_ρ, Collagen degradation	$\delta_\rho \approx 0.3k$	Aumailley et al. (1982)
a_z, Collagenase production	$a_z \approx 3.37 \times 10^{-9}$ ng/cell day	Oono et al. (2002), Dale et al. (1996), TW
ζ, Relative collagenase production by myofibroblasts	$\zeta \approx 2$	TW

Table 1 (*Continued*)

| Parameter	Range	Reference
b_z, Inhibition of collagenase production by TGFβ	$b_z \approx 3/\beta_0$	Overall et al. (1991)
δ_z, Collagenase decay	$\delta_z \approx 0.3616$/day	Overall et al. (1991)
s, Tethering coefficient	$s \approx 1$	Olsen et al. (1995)
μ, Viscosity	$\mu \approx O(10)$	Olsen et al. (1995)
Y, Elastic modulus	$10 < Y < 300$ N	Silver et al. (2001), Genzer and Groenewold (2006)
τ, Fibroblast cell traction	$1 < \tau < 3$ μN/cell	Wrobel et al. (2002), Fray et al. (1998)
ξ, Ratio of myofibroblast to fibroblast cell traction	$\xi \approx 2$	Wrobel et al. (2002)
β_0, Initial TGFβ concentration	$\beta_0 \approx 275$ ng/mL	Yang et al. (1999)
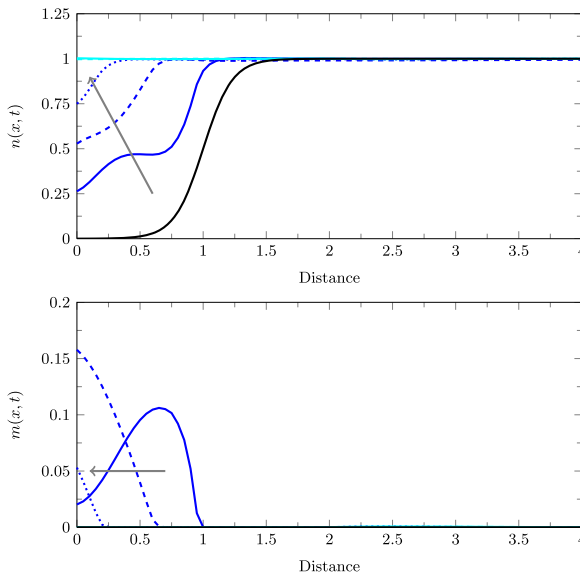
Fig. 1 Model predictions for the fibroblast and myofibroblast densities. *Black solid curves* represent the initial condition of each species. *Arrows* indicate the direction of increasing time, with each curve representing an increment in time of 6 days out to 30 days. The computational domain is 10 semi-wound lengths, so that $0 < x < 10$. In order to show behaviour in the wound more clearly, only the domain $0 < x < 4$ is shown. Parameter values are given by $D_n = 0.001$, $\chi = 0.003$, $a_\chi = 0.2$ $\alpha = 3$, $a_{n\beta} = 2$, $r = 0.832$, $a_{m\beta} = 2$, $a_{m\sigma} = 0.42$, $\theta_m = 0.9$, $\theta_{mm} = 1.64$, $D_\beta = 0.025$, $a_\beta = 0.1$, $\eta = 2$, $b_b = 5$, $a_{\beta z} = 0.25$, $a_{\beta m} = 0.21$, $\delta_\beta = 0.35$, $D_P = 0.0029$, $a_P = 2.4$, $\delta_P = 2.4$, $\delta_{Pn} = 20$, $\kappa = 0.1$, $\pi = 2$, $a_{\rho\beta} = 2$, $\omega = 0.2$, $\zeta = 2$, $b_z = 5$, $s = 1$, $\mu = 20$, $E = 10$, $\lambda = 2.2$, $\xi = 2$

wound contraction and further fibroblast activation. Fibroblasts continue to transform to myofibroblasts, with the greatest density of myofibroblasts occurring where the elastic stress is highest. There is a small level of myofibroblast activation predicted

Fig. 2 Model predictions for the TGFβ and PDGF concentration. *Black solid curves* represent the initial condition of each species. *Arrows* indicate the direction of increasing time, with each curve representing an increment in time of 6 days out to 30 days. Parameter values are the same as Fig. 1
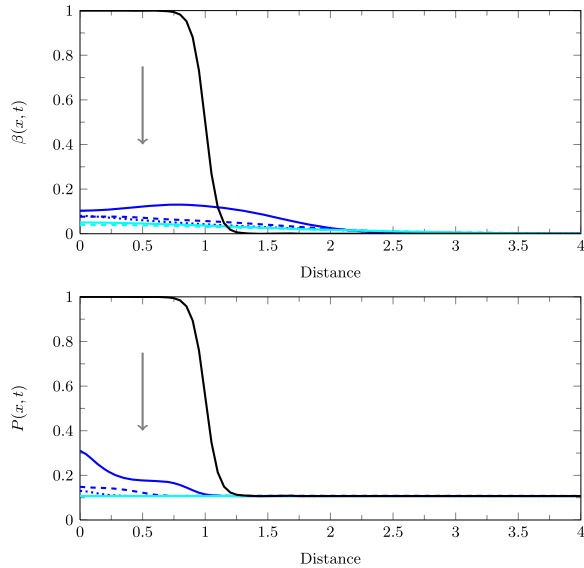
outside the wound due to small elastic stresses and the presence of a small concentration of TGFβ there. At long time, both the elastic stress and TGFβ tend to zero, and so the myofibroblast density tends to zero also (results not shown).

3.3 Transforming Growth Factor β

TGFβ appears early in the wound healing process as a result of the inflammatory cascade. Since there is no active TGFβ in unwounded dermis, the TGFβ concentration is initially zero outside the wound space (see Fig. 2). The concentration of TGFβ within the wound is gradually depleted through natural decay. However, both fibroblasts and myofibroblasts produce TGFβ and it can be activated through cleavage by collagenase and from latent stores in the matrix by myofibroblasts. As a result, the decay of TGFβ is quickly stemmed, which explains why it is still present at day 30, and why there is an increase in TGFβ around the wound boundary for early times. At later times, the TGFβ concentration tends to zero throughout. We note that our expression for myofibroblast activation of TGFβ from local matrix stores assumes that fibroblasts and myofibroblasts bind more TGFβ to the ECM than can be activated when the myofibroblasts contract the collagen fibers. Hence, it is assumed that there is always a supply of TGFβ attached to the matrix available for activation, which may or may not be accurate.

3.4 PDGF

Platelets release huge quantities of PDGF early in repair, yielding the significantly higher concentration of PDGF inside the wound initially. As fibroblasts repopulate the wound space, fibroblast-mediated depletion of PDGF occurs until the PDGF concentration attains unwounded levels within the lesion.

Fig. 3 Model predictions for the collagen density, collagenase concentration, and collagen displacement. *Black solid curves* represent the initial condition of each species. *Arrows* indicate the direction of increasing time, with each curve representing an increment in time of 6 days out to 30 days. It should be noted, however, that $u(x, t)$ increases during the first 6 days. Parameter values are the same as Fig. 1. We note that the computational domain is ten semi-wound lengths, such that $0 < x < 10$, and that the displacement, u, does tend to zero at the right-hand boundary
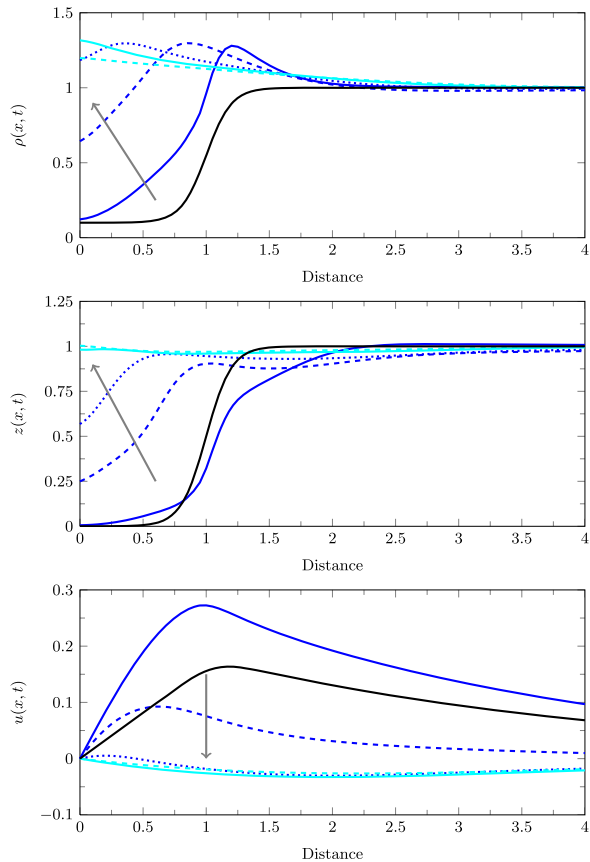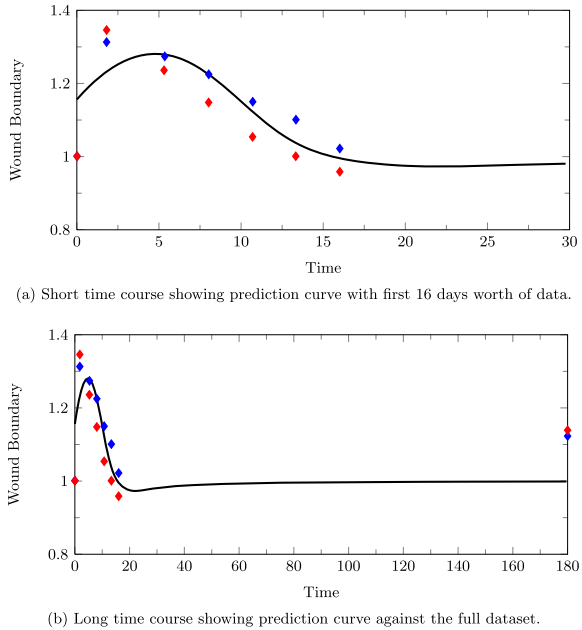
3.5 Collagen

Initially, we assume that there is a low density of collagen within the wound while the density is at unwounded levels outside. Synthesis of collagen by both fibroblasts and myofibroblasts is the primary source of collagen. The wound is largely healed as a result of infilling, consistent with experiments on human dermal repair (Catty 1965). Collagen production by cells is upregulated by the presence of TGFβ. This fact, combined with the near-unwounded levels of fibroblasts and the high density of myofibroblasts, gives rise to excess collagen within the wound space; as we see, the collagen profile is very similar to the TGFβ profile. While not shown in Fig. 3, re-modelling by the fibroblasts at later times ensures that the collagen density ultimately tends to unwounded levels throughout the domain.

3.6 Collagenase

It is assumed that there is no collagenase within the wound initially, but that the collagenase is at unwounded levels outside. The collagenase concentration inside the lesion decreases at early times, which can be attributed to the large early retraction.

Fig. 4 The wound boundary prediction from our model is the *solid curve*. Two series of data points for human wound closure were obtained by Catty (1965). Except for at $t = 2$ days and 180 days, the Series A data points lie below the corresponding data points for Series B. The daily collection of wound boundary data ceased at day 16 post wounding. One further measurement was made at 6 months. Parameter values are the same as Fig. 1

(a) Short time course showing prediction curve with first 16 days worth of data.

(b) Long time course showing prediction curve against the full dataset.

As the cells synthesize collagenase, the production is inhibited by the presence of TGFβ, and collagenase secretion is lowest at the wound centre where the TGFβ concentration is highest. Collagenase levels eventually tend to unwounded levels. Since collagenase is non-zero at steady state, this implies that there is a balance reached between collagenase production and degradation at steady state. Furthermore, this suggests that there is continuous turnover of ECM in unwounded tissue, which is consistent with clinical observations (Roberts et al. 1990).

3.7 Wound Boundary

The current position of the wound boundary can be obtained by finding the point x_{wb}, where the dimensionless displacement satisfies

$$x_{\mathrm{wb}} = 1 + u(x_{\mathrm{wb}}, t). \tag{17}$$

Thus, x_{wb} represents the material point that was located at $x = 1$ when $t = 0$. The movement of the wound boundary is represented by the black curves in Fig. 4.

Figures 4a and 4b show the comparison between our predicted curve and the data obtained by Catty (1965) for human wounds. Our model predicts the large initial retraction, and slow contraction of the wound, agreeing well with the data. However, our model does not predict an initial scaled wound boundary position of unity. This is because our model begins after the almost-instantaneous retraction that occurs following injury. In addition, whilst our model does predict a small late retraction, we did not observe the large late retraction seen by Catty. Apart from these few data points, however, good agreement is seen between the data of Catty (1965) and our

Fig. 5 The wound boundary prediction from our model is the *black curve*, and has been scaled respective to the initial wound size. Data showing the contractile phases of wound closure were obtained from McGrath and Simon (1983) for circular (●), small square (+) and large square (×) wounds, respectively. Parameter values are the same as Fig. 1
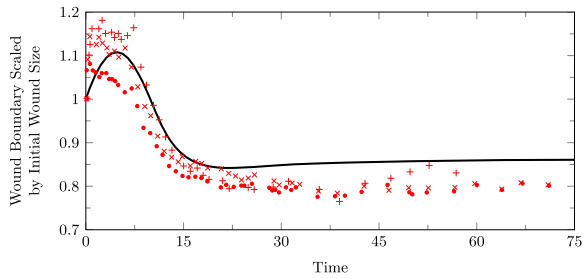

Table 2 Data reproduced from Catty (1965) together with the corresponding predictions from our model. The healed model value at day 16 corresponds to the point when Catty terminated the daily measurements, while 'max' represents the predicted maximum contraction from the model at day 22. Series A contained 11 patients, while Series B had 9 patients. Pre-excision refers to the area to be removed from the patient, actual area indicates the area of tissue actually excised, post-excision is the area of the wound after the retraction or expansion of the wound following removal of the tissue, healed refers to the day 16 values while 6 months values refer to the amount of retraction observed 6 months following wounding, as measured by Catty and predicted by the model

Series	Actual Area (sq. cm.)	Pre-Excision	Post-Excision	Healed		Six Months
A	1.01	1.000	1.316	1.041		1.123
B	1.07	1.000	1.343	0.960		1.139
Model	–	1.000	1.281	Day 16	Max	0.999
				0.995	0.973	

prediction curves. This is especially true when examining the early expansion and contraction measurements.

Table 2 gives the values for expansion (or retraction), contraction and late retraction observed by both Catty and colleagues and our simulation curve. We note that our model did not predict the maximum retraction to occur at day 16, but rather at day 22. Hence, we give two "healed" estimates: the predicted day 16 result and the value obtained at the maximum contraction (day 22). However, the day 16 and 22 predictions differ very little and both indicate that the majority of contraction occurs during the first 3 weeks of wound repair. These predictions are very similar to those obtained by Catty (1965), aside from the post six months column. This again confirms that for the proliferative stage of wound repair that we are modelling, good agreement is seen between the model predictions and the data.

We note from Table 2 that the expansion and healed values are comparable. With regard to the amount of late retraction predicted by our model, we were not able to obtain the large retraction observed by Catty (1965). However, the purpose of our model was to simulate the proliferative phase of wound repair, and so it is really only appropriate for the first 30 days of wound repair; during this time, the model compares well with the experimental data.

In Fig. 5, we consider the same simulation curve, but in this case we compare our prediction of wound closure qualitatively against the McGrath and Simon (1983)

data for rat dermal repair. Rat wounds exhibit far greater contraction than do human dermal injuries. Consequently, we scale the data from McGrath and Simon (1983) using

$$y_{\text{scaled}} = \frac{5}{7} + \frac{2}{7} y_{\text{data}}, \tag{18}$$

so that comparable contraction is observed in both the data and the model predictions. This scaling is sensible as human wounds heal with almost a third the contraction observed in rat dermal repair.

We see from the figure that the initial retraction, contraction, permanent contraction and late retraction observed in the data of McGrath and Simon (1983) are all predicted by our model. Hence, not only does our model correctly predict the closure of human dermal wounds, it reproduces all the phenomena found in murine dermal wound closure. Therefore, we believe this model represents a reasonable description of the closure of dermal wounds.

4 Discussion

Learning about how chemical mediators change the behaviour of cells is essential if we are to understand successful wound healing and chronic wound healing. This paper develops a mathematical model of wound healing that takes into account recent experimental observations about two of the critical cell types in wounds: fibroblasts and their more contractile form, myofibroblasts. The observation that the conversion from fibroblasts to myofibroblasts requires both the presence of TGFβ and tissue tension at the cellular level can only be modelled if a mechanical approach is taken. Here, we have extended the models of Tranquillo–Murray and Olsen and coworkers to include this activation process. The parameters in the model equations have been established from the published literature where possible and the model predictions obtained by solving the governing set of partial differential equations numerically. The predictions have been compared with two sets of experimental observations: Catty's observations on humans (Catty 1965) and Simon and McGrath's experiments on rats (McGrath and Simon 1983). In both cases, the model predictions are consistent with the experiments.

Our model predicts the large retraction and subsequent contraction seen during the first month of human dermal repair, a phenomenon not considered in previous mechanochemical representations of wound healing. The large retraction is due to the absence of fibroblasts and collagen within the wound space, and the contraction occurs following infilling as the fibroblasts and myofibroblasts contract the newly formed collagen matrix.

Previous researchers have not addressed the manner in which TGFβ and tissue mechanics inform the activation of fibroblasts to myofibroblasts. Our model predicts that it is the elimination of TGFβ from the system, together with the reduction in local tension, that reduces the presence of myofibroblasts toward the end of the proliferative phase.

Our model investigates the complex interactions between cells, TGFβ and collagenase in the regulation of collagen expression. During the period in which the

TGFβ concentration is high, we found that collagen expression is heightened within the wound space. This can be attributed to both the presence of myofibroblasts and to the increased production of collagen by both fibroblasts and myofibroblasts in the presence of TGFβ. The myofibroblast density and TGFβ concentration tend to zero, but remodelling of the collagen network by fibroblasts and collagenase continues, so that the collagen density approaches healed levels across the wound space.

While this paper has concentrated on successful "normal" dermal wound healing, we see that this modelling framework could be extended in a number of ways. Excessive wound contraction in humans can be both disfiguring and can cause mobility problems if the contractures occur over joints in the hands or at the elbow. These are often associated with severe burns and we are exploring strategies to reduce contractures by increasing the death rate of myofibroblasts and nullifying the effects of TGFβ. Another extension is to incorporate the role of oxygen in the wound healing process. McGrath and Emery (1985) showed that the contraction in a rat wound was slowed when angiogenesis (new blood vessel growth) was impeded. We intend to couple the current system with a representation of angiogenesis to examine the combined effect of inflammation, fibroplasia, and angiogenesis in wound closure.

Wound geometry and depth are known to play a role in the rapidity of repair (Billingham and Russell 1956; McGrath and Simon 1983). Thus, one could extend the current model to two dimensions to investigate the impact of these phenomena on healing. Another possibility would be to analyse how repair is affected by wound debridement, in which the granulation tissue and other constituents are removed. Alternatively, it would be possible to examine the effect of addition or removal of TGFβ. Indeed, Ferguson and O'Kane (2004) found that addition of different isoforms of TGFβ can improve or exacerbate repair. Therefore, one may wish to distinguish between the TGFβ isoforms instead of using a single generic independent variable to represent the total concentration of TGFβ.

As our model includes TGFβ, collagenase and collagen, it can be used to investigate wound healing pathologies, such as keloid development, where the interactions between these three species are significant. In future work, we will examine the formation of keloids using an extension of this model. Another type of pathological scarring that warrants attention is scar hypertrophy. In the Aarabi et al. (2007) experiments in murine tissue, scar hypertrophy was elicited when the wound was held open. In our model, the undamaged dermal tissue/wound boundary was free to move. However, by restricting this assumption, our framework could be modified to model this setup.

We see an important aspect of wound healing that has not been modelled in detail is the interaction between the epidermal cells that migrate into the wound and the cells of the underlying dermis. While some early work has addressed this issue (see Chaps. 9 and 10 of Murray 2003), there is a considerable body of recent experimental literature that elucidates the cross-talk between these cell types. The framework in this paper could be extended to include an invading epidermal layer although the mechanics of this interaction would need to be informed by further experimental data.

In summary, our model has been able to simulate the course of human dermal repair using carefully determined parameter values. This model incorporates a detailed

representation of cytokine kinetics coupled with the intricate interactions between the cellular, extracellular, and chemical species. We addressed the manner by which TGFβ and tissue mechanics cooperate to activate fibroblasts to myofibroblasts. The results are consistent with experimental data, with the wound boundary curve shown to ably predict the human wound contraction data of Catty (1965) and the scaled rat contraction experiments of McGrath and Simon (1983), with all of the essential features of wound contraction being well matched. Moreover, our model successfully simulates the heterogeneous nature of the mechanical environment and could be extended to explore the effects of elevated skin tension on hypertrophic scarring and other pathologies.

Appendix A: Non-dimensional Equations

Applying the following non-dimensionalization,

$$\hat{N} = \frac{r}{\theta_{nn}}, \qquad \hat{B} = \beta_0, \qquad \hat{Z}^2 = \frac{a_z k \hat{N}^2}{\delta_\rho \delta_\zeta}, \qquad \hat{R} = \frac{k\hat{N}}{\delta_\rho \hat{Z}}, \qquad \hat{V} = \frac{L}{T},$$

$$\bar{D}_n = \frac{D_n T}{L^2}, \qquad \bar{\alpha} = \alpha B T, \qquad \bar{a}_{n\beta} = a_{n\beta} \hat{B}, \qquad \bar{a}_n = rT, \qquad \bar{a}_{m\sigma} = a_{m\sigma} T,$$

$$\bar{a}_{m\beta} = a_{m\beta} \hat{B}, \qquad \bar{\theta}_m = \theta_m T, \qquad \bar{\theta}_{mm} = \theta_{mm} \hat{N} T, \qquad \bar{a}_\beta = a_\beta \hat{N} T, \qquad \bar{b}_\beta = b_\beta \hat{B},$$

$$\bar{D}_\beta = \frac{D_\beta T}{L^2}, \qquad \bar{\eta} = \eta, \qquad \bar{a}_{\beta m} = \frac{a_{\beta m} \hat{N} \hat{R} T}{\hat{B}}, \qquad \bar{a}_{\beta z} = a_{\beta z} \hat{Z} T, \qquad \bar{\delta}_\beta = \delta_\beta T,$$

$$\bar{K} = \frac{k\hat{N}T}{\hat{R}}, \qquad \bar{a}_{\rho\beta} = a_{\rho\beta} \hat{B}, \qquad \bar{\omega} = \delta_\zeta T, \qquad \bar{b}_\zeta = b_\zeta \hat{B}, \qquad \bar{s} = sL^2,$$

$$\bar{E} = E, \qquad \bar{\mu} = \frac{\mu}{\hat{R}T}, \qquad \bar{\lambda} = \lambda \hat{N}, \qquad \bar{\xi} = \xi, \qquad \bar{\pi} = \pi,$$

$$\bar{\zeta} = \zeta, \qquad \hat{P} = P_0, \qquad \bar{\chi} = \frac{\chi T}{L^2 \hat{P}}, \qquad \bar{a}_\chi = \frac{a_\chi}{\hat{P}}, \qquad \bar{D}_P = \frac{D_P T}{L^2},$$

$$\bar{a}_P = \frac{a_P T}{\hat{P}}, \qquad \bar{\delta}_P = \delta_P T, \qquad \bar{\delta}_{Pn} = \delta_{Pn} T \hat{N},$$

and dropping bars, we obtain the following non-dimensional equations:

$$\frac{\partial n}{\partial t} + \frac{\partial}{\partial x}(nv) = \frac{\partial}{\partial x}\left[D_n \frac{\partial n}{\partial x} - \frac{\chi n}{(a_\chi + P)^2} \frac{\partial P}{\partial x} \right]$$

$$+ r(1 + a_{n\beta}\beta)n(1 - n - m) - \alpha\sigma^{+}\beta n, \tag{19}$$

$$\frac{\partial m}{\partial t} + \frac{\partial}{\partial x}(mv) = m\big(a_{m\sigma}\sigma^{+}(1 + a_{m\beta}\beta) - \theta_m - \theta_{mm}(n + m)\big) + \alpha\sigma^{+}\beta n, \tag{20}$$

$$\frac{\partial \beta}{\partial t} + \frac{\partial}{\partial x}(\beta v) = D_\beta \frac{\partial^2 \beta}{\partial x^2} + \frac{a_\beta \beta(n + \pi m)}{1 + b_\beta \beta} + a_{\beta m}m\rho + a_{\beta z}z\beta - \delta_\beta \beta, \tag{21}$$

$$\frac{\partial P}{\partial t} + \frac{\partial}{\partial x}(Pv) = D_p \frac{\partial^2 P}{\partial x^2} + a_P - \delta_P P - \delta_{Pn}nP, \tag{22}$$

$$\frac{\partial \rho}{\partial t} + \frac{\partial}{\partial x}(\rho v) = \kappa\big((n + \eta m)(1 + a_{\rho\beta}\beta) - \rho z\big), \tag{23}$$

$$\frac{\partial z}{\partial t} + \frac{\partial}{\partial x}(zv) = \omega\left(\frac{\rho(n + \zeta m)}{1 + b_z \beta} - z\right), \tag{24}$$

$$s\rho u = \frac{\partial}{\partial x}\left(\sigma + \mu \frac{\partial v}{\partial x} + \psi\right), \tag{25}$$

$$\sigma = E\rho \frac{\partial u}{\partial x}, \tag{26}$$

$$\psi = \lambda\rho(n + \xi m), \tag{27}$$

$$v = \frac{\partial u}{\partial t}. \tag{28}$$

Appendix B: Initial Conditions

The following represent the scaled initial conditions employed in this model:

$$n(x, 0) = \frac{1}{2}\left\{1 + \tan\left(\frac{x - L}{\epsilon_n}\right)\right\}, \tag{29}$$

$$m(x, 0) = 0, \tag{30}$$

$$\beta(x, 0) = \frac{1}{2}\left\{1 - \tan\left(\frac{x - L}{\epsilon_\beta}\right)\right\}, \tag{31}$$

$$P(x, 0) = \frac{1}{2}\left\{(P_{ss} + P_{in}) + (P_{ss} - P_{in})\tan\left(\frac{x - L}{\epsilon_\rho}\right)\right\}, \tag{32}$$

$$\rho(x, 0) = \frac{1}{2}\left\{(1 + \rho_{in}) + (1 - \rho_{in})\tan\left(\frac{x - L}{\epsilon_\rho}\right)\right\}, \tag{33}$$

$$z(x, 0) = \frac{1}{2}\left\{1 + \tan\left(\frac{x - L}{\epsilon_z}\right)\right\}, \tag{34}$$

where $\epsilon_n = 0.1$, $\epsilon_\beta = \epsilon_\rho = \epsilon_z = 0.4$, controlling the steepness across the boundary, $\rho_{in} = 0.1$, the initial scaled collagen density within the wound space, P_{ss} is the steady-

state value for PDGF in the presence of fibroblasts, given by $P_{ss} = a_P/(\delta_P + \delta_{Pn}n)$, $P_{in} = a_P/\delta_P$, is the steady-state value for PDGF in the absence of fibroblasts, and $L = 1$, the scaled initial position of the wound boundary.

Appendix C: Parameter Estimation

First, we estimate values for the scalings used to non-dimensionalize the variables:

L: A typical length scale for acute dermal wounds is 1 cm.
T: A typical length scale for time is days. Hence, $T = 1$ day.
r: In Murphy et al. (2011) we estimate fibroblast proliferation to be $r = 0.832$/day.
θ_{nn}^{-1}: The carrying capacity of fibroblasts is known to be approximately 10^6 cells/mL
   (Vande Berg et al. 1989). Hence, we take $\theta_{nn}^{-1} = 10^6$ cells/mL.
k/δ_ρ: It is known that 30% of newly synthesized collagen is degraded (Aumailley
   et al. 1982). Hence, $\delta_\rho = 0.3k$, such that $k/\delta_\rho = 3.33$. Bahar et al. (2004) estimates
   a collagen production rate of 1.75 pg/cell day.
β_0: Yang et al. (1999) found the initial concentration of TGFβ in the wound to be
   275 ng/mL. Hence, we take $\beta_0 = 275$ ng/mL.
P_0: Olsen et al. (1995) states that PDGF is stored in platelets at concentrations of
   approximately 15–50 ng/mL. Olsen et al. (1995), Haugh (2006) and Schugart et al.
   (2008) all propose an initial PDGF concentration of $P_0 = 10$ ng/mL, which we
   adopt.

We can now apply the following non-dimensionalization:

$$\bar{x} = \frac{x}{L}, \qquad \bar{t} = \frac{t}{T}, \qquad \bar{n} = \frac{n}{\hat{N}}, \qquad \bar{m} = \frac{m}{\hat{N}}, \qquad \bar{P} = \frac{P}{P_0},$$

$$\bar{\rho} = \frac{\rho}{\hat{R}}, \qquad \bar{z} = \frac{z}{\hat{Z}}, \qquad \hat{\beta} = \frac{\beta}{\beta_0} \qquad \bar{u} = \frac{u}{L}, \qquad \bar{v} = \frac{Tv}{L}.$$

The values for the remaining dimensional parameters are as follows. app D_n: Experiments by Sillman et al. (2003) found that fibroblasts derived from normal human dermal wounds migrate at an average velocity of 0.23–0.36 µm/min. This gives a range for the minimum wavespeed of $0.00033 < D_n < 0.001$ cm²/day. We choose the upper limit of $D_n = 0.001$ cm²/day.

χ: Olsen et al. (1995) recognized that the chemotactic coefficient should predominate over the random diffusive flux. In the absence of quantitative studies, Haugh (2006) and Monine and Haugh (2008) propose that the chemotactic coefficient is three times the magnitude of the diffusivity. We chose a value for $D_n = 0.001$ cm²/day, and controlling for the PDGF density ($P_0 = 10$ ng/mL), this gives a chemotaxis coefficient of $\chi = 0.03$ ng/cm day.
a_χ: Olsen et al. (1995) notes that experimental data suggests that the half-maximal response of fibroblasts to PDGF-mediated chemotaxis occurs at a concentration of 2 ng/mL. Thus, we take $a_\chi = 2$ ng/mL.
$a_{n\beta}$: Strutz et al. (2001) found TGFβ to increase fibroblast proliferation by 2–3 times. Hence, we assume that $a_{n\beta} = 2/\beta_0$.

α: Desmouliere et al. (1993) found that culturing fibroblasts in the presence of TGFβ increased the percentage of cells expressing α-SMA from 7.5% to 45.3%, representing an activation of 37.8% of fibroblasts, and is consistent with other estimates (Masur et al. 1996; Moulin et al. 1996). This experiment occurred over a one week period, with a TGFβ dose of 5–10 ng/mL. This gives a range for the activation of $0.0054 < \alpha < 0.0108$/day (ng/mL). We choose the upper limit of $\alpha = 0.0108$/day (ng/mL).

$a_{m\sigma}$: The myofibroblast growth rate is lower than that of normal dermal fibroblasts, with myofibroblast growth approximately 50% that of fibroblasts (Vande Berg et al. 1989). Thus, we take the myofibroblast proliferation to be half that of fibroblasts, such that $a_{m\sigma} = 0.5r$.

$a_{m\beta}$: We assume that myofibroblasts experience the same increase in proliferation due to TGFβ as fibroblasts. Hence, $a_{m\beta} = a_{n\beta}$.

θ_m: The doubling time of fibroblasts is approximately 18 hours (Olsen et al. 1995). We assume that the doubling time of myofibroblasts is the same as that for fibroblasts. Hence, this gives a natural cell death rate for the myofibroblasts of $\theta_m \approx 0.90$.

θ_{mm}: As myofibroblasts are roughly twice the size of fibroblasts (Masur et al. 1996), we assume that myofibroblasts have half the carrying capacity of fibroblasts, i.e., $\theta_{mm} = 2\theta_{nn} = (0.5 \times 10^6)^{-1}$.

D_β: Using known estimates of the molecular weight of epidermal growth factor (EGF) and TGFβ (Cell Signaling Technology 2010) and the diffusivity of epidermal growth factor (Thorne et al. 2004), we were able to determine the diffusivity of TGFβ using the Stokes–Einstein formula, such that $D_\beta \approx 0.0254$ cm^2/day.

a_β: Experiments by Wang et al. (2000) give the range for TGFβ production by fibroblasts as $0.125 < a_\beta < 0.525 \times 10^{-6}$ ng/(cell day). We choose the lower limit, such that $a_\beta = 0.125 \times 10^{-6}$ ng/(cell day).

η, π, ζ: On a percentage basis, myofibroblasts produce roughly twice the collagen that is synthesized by fibroblasts (Kim and Friedman 2009; Moulin et al. 1998; Olsen et al. 1995). Hence, we choose $\eta = 2$. There is a similar trend for myofibroblast synthesis of TGFβ (see Kim and Friedman, 2009) and based on these relations, we assume the same is true for myofibroblast production of collagenase. Hence, $\pi = \zeta = \eta = 2$.

b_β: Using estimates from Dale et al. (1995), inhibition of TGFβ synthesis is assumed to be $b_\beta = 5/\beta_0$.

$a_{\beta z}$: Using order of magnitude approximation, we estimate the activation of TGFβ by collagenase to be $\sim O(0.1)$ when non-dimensionalized. Thus, $a_{\beta z} = 0.0014$ mL/ng day.

$a_{\beta m}$: We assume that the amount of TGFβ activated from matrix stores is of the same order of magnitude as the amount of TGFβ activated by collagenase following non-dimensionalization, i.e., $O(0.1)$. Hence, we estimate the activation of TGFβ by myofibroblasts to be 4.37×10^{-9} mL day/cell.

δ_β: The TGFβ decay rate was estimated from the exponential phase of the data from Yang et al. (1999), giving a rate of $\delta_\beta \approx 0.354$/day.

D_P: Haugh (2006) states that the diffusion coefficient for PDGF in aqueous solution is estimated at 10^{-6} cm^2/s (0.0864 cm^2/day), or twice the value taken by Olsen et al. (1995). However, Haugh (2006) then states that diffusion of cytokines in tissue is

much slower than in solutions, and that the diffusion of PDGF in the dermis is approximately one thirtieth of its value in solution. Thus, the diffusion coefficient for PDGF is taken to be $D_P = 0.00288$ cm^2/day.

δ_P: Olsen et al. (1995), Haugh (2006) and Monine and Haugh (2008) all consider PDGF decay to be $O(1)$/day. We use the value given by Haugh (2006) and Monine and Haugh (2008) of $\delta_P = 2.4$/day.

a_P: The range suggested by Olsen et al. (1995) for the production of PDGF (depending upon the cellular density, which ranges from 10^4–10^6) is 4–400 ng/cm^3 day, while Haugh (2006) proposes limits of 4.8–48 ng/cm^3/day, which we see encapsulates the lower end of the parameter range suggested by Olsen et al. (1995). Both Haugh (2006) and Monine and Haugh (2008) use the value of $a_P = 24$ ng/cm^3/day so that the production rate of PDGF balances the degradation rate in the absence of fibroblasts (where $a_P = \delta_P P_0$).

δ_{Pn}: Haugh (2006) estimates the range for the fibroblast consumption of PDGF to be $2.4 < \delta_{Pn} < 48$/day, and proposes that a reasonable value for this parameter is 2.4/day, a value which Monine and Haugh (2008) also adopts. After accounting for the cell density, we obtain an estimate for fibroblast PDGF consumption of $\delta_{Pn} = 2.4$ cm^3/cell/day

$a_{\rho\beta}$: Eickelberg et al. (1999) found a 2–3-fold increase in collagen expression by human lung fibroblasts in the presence of TGFβ. We assume that TGFβ induces a similar increase in collagen production by dermal fibroblasts. Hence, we estimate that $a_{\rho\beta} = 2/\beta_0$.

a_z: Oono et al. (2002) estimates the collagenase accumulation over one day to be 5–35 ng/mL. Using this value, and the steady state values for collagen density ($\sim$15 μg/mg, Dale et al. 1996), fibroblasts (r/θ_{nn}), collagenase ($\sim$0.1 ng/mL, determined from Dale et al. 1996) and recognizing that the velocity, myofibroblast density and TGFβ concentration are zero, we may substitute into (16) and determine a value for collagenase production. We estimate its value to be $a_z = 3.37 \times 10^{-9}$ ng/cell/day.

b_z: Overall et al. (1991) found a reduction of 66–75% of collagenase synthesis in the presence of TGFβ. This gives an estimate of $b_z = 3/\beta_0$.

δ_z: Overall et al. (1991) estimate the half-life of MMP-2 as 46 hours. We assume that collagenase (MMP-1) has the same half-life, giving a decay rate of 0.3616/day.

s: Following Tranquillo and Murray (1992), Olsen et al. (1995) and Javierre et al. (2009), we consider a tethering coefficient of $s = 1$.

μ: We follow Olsen et al. (1995) and Javierre et al. (2009), and choose μ such that its non-dimensional value is 20.

E: Estimates of E range from 1–300 N/cm^2 (Silver et al. 2001; Genzer and Groenewold 2006). We consider an area of approximately 1 cm^2, which gives a range of E of $10 < E < 300$ N. We use the lower limit, such that $E = 10$ N.

τ: In Murphy et al. (2011), we estimated a range for τ of $1 < \tau < 3$ μN/cell. Hence, we consider a value of $\tau = 2.65$ μN/cell, consistent with Fray et al. (1998) and Wrobel et al. (2002).

ξ: Wrobel et al. (2002) found that myofibroblasts can apply up to twice the cell traction force generated by fibroblasts. Hence, we choose $\xi = 2$.

References

Aarabi, S., Bhatt, K. A., Shi, Y., Paterno, J., Chang, E. I., Loh, S. A., Holmes, J. W., Longaker, M. T., Yee, H., & Gurtner, G. C. (2007). Mechanical load initiates hypertrophic scar formation through decreased cellular apoptosis. *FASEB J.*, *21*, 3250–3261.

Aumailley, M., Krieg, T., Razaka, G., Müller, P. K., & Bricaud, H. (1982). Influence of cell density on collagen biosynthesis in fibroblast cultures. *Biochem. J.*, *206*, 505–510.

Bahar, M. A., Bauer, B., Tredget, E. E., & Ghahary, A. (2004). Dermal fibroblasts from different layers of human skin are heterogeneous in expression of collagenase and types I and III procollagen mRNA. *Wound Repair Regen.*, *12*, 175–182.

Barocas, V. H., & Tranquillo, R. T. (1997). An anisotropic biphasic theory of tissue-equivalent mechanics: the interplay among cell traction, fibrillar network deformation, fibril alignment, and cell contact guidance. *J. Biomech. Eng.*, *119*, 137–145.

Billingham, R. E., & Medawar, P. B. (1955). Contracture and intussusceptive growth in the healing of extensive wounds in mammalian skin. *J. Anat.*, *89*, 114–123.

Billingham, R. E., & Russell, P. S. (1956). Studies on wound healing, with special reference to the phenomenon of contracture in experimental wounds in rabbits' skin. *Ann. Surg.*, *144*, 961–981.

Brown, B. C., McKenna, S. P., Siddhi, K., McGrouther, D. A., & Bayat, A. (2008). The hidden cost of skin scars: quality of life after skin scarring. *J. Plast. Reconstr. Aesthet. Surg.*, *61*, 1049–1058.

Brown, B. C., Moss, T. P., McGrouther, D. A., & Bayat, A. (2010). Skin scar preconceptions must be challenged: importance of self-perception in skin scarring. *J. Plast. Reconstr. Aesthet. Surg.*, *63*, 1022–1029.

Catty, R. H. C. (1965). Healing and contraction of experimental full-thickness wounds in the human. *Br. J. Surg.*, *52*, 542–548.

Inc. Cell Signaling Technology (2010). Growth factors & cytokines. Published online at Cell Signaling Technology, URL: http://www.cellsignal.com/products/8916.html.

Chakraborti, S., Mandal, M., Das an A. Mandal, S., & Chakraborti, T. (2003). Regulation of matrix metalloproteinases: an overview. *Mol. Cell. Biochem.*, *253*, 269–285.

Cook, J. (1995). *A mathematical model for dermal wound healing: wound contraction and scar formation.* PhD thesis, University of Washington.

Cotran, R. S., Kumar, V., & Collins, T. (1999). *Robbins pathologic basis of diseases* (6th ed.). Philadelphia: Saunders.

Cumming, B. D., McElwain, D. L. S., & Upton, Z. (2010). A mathematical model of wound healing and subsequent scarring. *J. R. Soc. Interface*, *7*, 19.

Dale, P. D., Olsen, L., Maini, P. K., & Sherratt, J. A. (1995). Travelling waves in wound healing. *Forma*, *10*, 205–222.

Dale, P. D., Sherratt, J. A., & Maini, P. K. (1996). A mathematical model for collagen fibre formation during foetal and adult dermal wound healing. *Proc. Biol. Sci.*, *263*, 653–660.

Dale, P. D., Sherratt, J. A., & Maini, P. K. (1997). Role of fibroblast migration in collagen fiber formation during fetal and adult dermal wound healing. *Bull. Math. Biol.*, *59*, 1077–1100.

Dallon, J. C., & Sherratt, J. A. (1998). A mathematical model for fibroblast and collagen orientation. *Bull. Math. Biol.*, *60*, 101–129.

Dallon, J. C., Sherratt, J. A., & Maini, P. K. (1999). Mathematical modelling of extracellular matrix dynamics using distrete cells: fiber orientation and tissue regeneration. *J. Theor. Biol.*, *199*, 449–471.

Dallon, J. C., Sherratt, J. A., & Maini, P. K. (2001). Modeling the effects of transforming growth factor-β on extracellular matrix alignment in dermal wound repair. *Wound Repair Regen.*, *9*, 278–286.

Desmouliere, A., Geinoz, A., Gabbiani, F., & Gabbiani, G. (1993). Transforming growth factor-β1 induces α-smooth muscle actin expression in granulation tissue myofibroblasts and in quiescent and growing cultured fibroblasts. *J. Cell Biol.*, *122*, 103–111.

Desmouliere, A., Redard, M., Darby, I., & Gabbiani, G. (1995). Apoptosis mediates the decrease in cellularity during the transition between granulation tissue and scar. *Am. J. Pathol.*, *146*, 56–66.

Desmouliere, A., Chaponnier, C., & Gabbiani, G. (2005). Tissue repair, contraction, and the myofibroblast. *Wound Repair Regen.*, *13*, 7–12.

Eickelberg, O., Kohler, E., Reichenberger, F., Bertschin, S., Woodtli, T., Erne, P., Perruchoud, A. P., & Roth, M. (1999). Extracellular matrix deposition by primary human lung fibroblasts in response to TGF-β1 and TGF-β3. *Am. J. Physiol. Lung Cell. Mol. Physiol.*, *276*, 814–824.

Enoch, S., & Leaper, D. J. (2007). Basic science of wound healing. *Surgery*, *26*, 31–37.

Enoch, S., Grey, J. E., & Harding, K. G. (2006). ABC of wound healing: Recent advances and emerging treatments. *Br. Med. J.*, *332*, 962–965.

Farahani, R. M., & Kloth, L. C. (2008). The hypothesis of 'biophysical matrix contraction': wound contraction revisited. *Int. Wound J.*, *5*, 477–482.

Ferguson, M. W. J., & O'Kane, S. (2004). Scar-free healing: from embryonic mechanisms to adult therapeutic intervention. *Philos. Trans. R. Soc. Lond. B*, *359*, 839–850.

Flegg, J. A., Byrne, H. M., & McElwain, D. L. S. (2010). Mathematical model of hyperbaric oxygen therapy applied to chronic diabetic wounds. *Bull. Math. Biol.*, *72*, 1867–1891.

Fray, T. R., Molloy, J. E., Armitage, M. O., & Sparrow, J. C. (1998). Quantification of single human dermal fibroblast contraction. *Tissue Eng.*, *4*, 281–291.

Genzer, J., & Groenewold, J. (2006). Soft matter with hard skin: from skin wrinkles to templating and material characterization. *Soft Matter*, *2*, 310–323.

Ghosh, K., Pan, Z., Guan, E., Ge, S., Liu, Y., Nakamura, T., Ren, Z.-D., Rafailovich, M., & Clark, R. A. F. (2007). Cell adaptation to a physiologically relevant ECM mimic with different viscoelastic properties. *Biomaterials*, *28*, 671–679.

Grinnell, F. (1994). Mini-review on the cellular mechanisms of disease—fibroblasts, myofibroblasts, and wound contraction. *J. Cell Biol.*, *124*, 401–404.

Grinnell, F. (2000). Fibroblast-collagen-matrix contraction: growth-factor signalling and mechanical loading. *Trends Cell Biol.*, *10*, 362–365.

Grinnell, F. (2003). Fibroblast biology in three-dimensional collagen matrices. *Trends Cell Biol.*, *13*, 264–269.

Hall, C. L. (2009). *Modelling of some biological materials using continuum mechanics*. PhD thesis, Queensland University of Technology.

Haugh, J. M. (2006). Deterministic model of dermal wound invasion incorporating receptor-mediated signal transduction and spatial gradient sensing. *Biophys. J.*, *90*, 2297–2308.

Herber, O. R., Schnepp, W., & Rieger, M. A. (2007). A systematic review on the impact of leg ulceration on patients' quality of life. *Health Qual. Life Outcomes*, *5*, 1–12.

Hinz, B. (2007). Formation and function of the myofibroblast during tissue repair. *J. Invest. Dermatol.*, *127*, 526–537.

Hinz, B. (2010). The myofibroblast: paradigm for a mechanically active cell. *J. Biomech.*, *43*, 146–155.

Hinz, B., Mastrangelo, D., Iselin, C. E., Chaponnier, C., & Gabbiani, G. (2001). Mechanical tension controls granulation tissue contractile activity and myofibroblast differentiation. *Am. J. Pathol.*, *159*, 1009–1020.

Javierre, E., Moreo, P., Doblare, M., & Garcia-Aznar, J. M. (2009). Numerical modeling of a mechano-chemical theory for wound contraction analysis. *Int. J. Solids Struct.*, *46*, 3597–3606.

Jenkins, G. (2008). The role of proteases in transforming growth factor-β activation. *Int. J. Biochem. Cell Biol.*, *40*, 1068–1078.

Kennedy, D. F., & Cliff, W. J. (1979). A systematic study of wound contraction in mammalian skin. *Pathology*, *11*, 207–222.

Kim, Y., & Friedman, A. (2009). Interaction of tumor with its micro-environment: a mathematical model. *Bull. Math. Biol.*, *72*, 1029–1068.

Masur, S. K., Dewal, H. S., Dinh, T. T., Erenburg, I., & Petridou, S. (1996). Myofibroblasts differentiate from fibroblasts when plated at low density. *Proc. Natl. Acad. Sci. USA*, *93*, 4219–4223.

McDougall, S., Dallon, J. C., Sherratt, J. A., & Maini, P. K. (2006). Fibroblast migration and collagen deposition during dermal wound healing: mathematical modelling and clinical implications. *Philos. Trans. R. Soc. A*, *364*, 1385–1405.

McGrath, M. H., & Emery, J. M. (1985). The effect of inhibition of angiogenesis in granulation tissue on wound healing and the fibroblast. *Ann. Plast. Surg.*, *15*, 105–122.

McGrath, M. H., & Simon, R. H. (1983). Wound geometry and the kinetics of wound contraction. *Plast. Reconstr. Surg.*, *72*, 66–72.

Monine, M. I., & Haugh, J. M. (2008). Cell population-based model of dermal wound invasion with heterogeneous intracellular signaling properties. *Cell Adhes. Migr.*, *2*, 137–145.

Monroe, D. M., Mackman, N., & Hoffman, M. (2010). Wound healing in hemophilia B mice and low tissue factor mice. *Thromb. Res.*, *125*, S74–S77.

Moulin, V., Castilloux, G., Jean, A., Garrel, D. R., Auger, F. A., & Germain, L. (1996). In vitro models to study wound healing fibroblasts. *Burns*, *22*, 359–362.

Moulin, V., Castilloux, G., Auger, F. A., Garrel, D. R., O'Connor-McCourt, M. D., & Germain, L. (1998). Modulated response to cytokines of humand wound healing myofibroblasts compared to dermal fibroblasts. *Exp. Cell Res.*, *238*, 283–293.

Moulin, V., Larochelle, S., Langlois, C., Thibault, I., Lopez-Vallé, C. A., & Roy, M. (2004). Normal skin wound and hypertrophic scar myofibroblasts have differential responses to apoptotic inductors. *J. Cell. Physiol.*, *198*, 350–358.

Murphy, K. E., Hall, C. L., McCue, S. W., & McElwain, D. L. S. (2011). A two-compartment mechanochemical model of the roles of transforming growth factor β and tissue tension in dermal wound healing. *J. Theor. Biol.*, *272*, 145–159.

Murray, J. D. (2003). *Interdisciplinary applied mathematics: Vol. 18. Mathematical biology II: spatial models and biomedical applications* (3rd ed.). Berlin: Springer.

Murray, J. D., Maini, P. K., & Tranquillo, R. T. (1988). Mechanochemical models for generating biological pattern and form in development. *Phys. Rep.*, *2*, 59–84.

Murray, J. D., Cook, J., Tyson, R., & Lubkin, S. R. (1997). Spatial pattern formation in biology: I. Dermal wound healing. II. Bacterial patterns. *J. Franklin Inst.*, *335*, 303–332.

Olsen, L., Sherratt, J. A., & Maini, P. K. (1995). A mechanochemical model for adult dermal wound contraction and the permanence of the contracted tissue displacement profile. *J. Theor. Biol.*, *17*, 113–128.

Olsen, L., Sherratt, J. A., & Maini, P. K. (1996). A mathematical model for fibro-proliferative wound healing disorders. *Bull. Math. Biol.*, *58*, 787–808.

Olsen, L., Sherratt, J. A., & Maini, P. K. (1997). A mechanochemical model for normal and abnormal dermal wound repair. *Nonlinear Anal.*, *30*, 3333–3338.

Olsen, L., Sherratt, J. A., & Maini, P. K. (1998). Spatially varying equilibria of mechanical models: application to dermal wound contraction. *Math. Biosci.*, *147*, 113–129.

Olsen, L., Maini, P. K., Sherratt, J. A., & Dallon, J. C. (1999). Mathematical modelling of anisotropy in fibrous connective tissue. *Math. Biosci.*, *158*, 145–170.

Oono, T., Shirafuji, Y., Huh, W.-K., Akiyama, H., & Iwatsuki, K. (2002). Effects of human neutrophil peptide-1 on the expression of interstitial collagenase and type I collagen in human dermal fibroblasts. *Arch. Dermatol. Res.*, *294*, 185–189.

Overall, C., Wrana, J., & Sodek, J. (1991). Transcriptional and post-transcriptional regulation of 72-kDa gelatinase/type IV collagenase by transforming growth factor-β1 in human fibroblasts. *J. Biol. Chem.*, *266*, 14064–14071.

Pettet, G., Chaplain, M. A. J., McElwain, D. L. S., & Byrne, H. M. (1996). On the role of angiogenesis in wound healing. *Proc. R. Soc., Biol. Sci.*, *263*, 1487–1493.

Ramtani, S. (2004). Mechanical modelling of cell/ECM and cell/cell interactions during the contraction of a fibroblast-populated collagen microsphere: theory and model simulation. *J. Biomech.*, *37*, 1709–1718.

Ramtani, S., Fernandes-Morin, E., & Geiger, D. (2002). Remodeled-matrix contraction by fibroblasts: numerical investigations. *Comput. Biol. Med.*, *32*, 283–296.

Roberts, A. B., Flanders, K. C., Heine, U. E., Jakowlew, S., Knodaiah, P., Kim, S.-J., & Sporn, M. B. (1990). Transforming growth factor-β: multifunctional regulator of differentiation and development. *Philos. Trans. R. Soc. Lond. B, Biol. Sci.*, *327*, 145–154.

Schugart, R. C., Friedman, A., Zhao, R., & Chandan, K. S. (2008). Wound angiogenesis as a function of tissue tension: a mathematical model. *Proc. Natl. Acad. Sci. USA*, *105*, 2628–2633.

Shultz, G. S., Ladwig, G., & Wysocki, A. (2005). Extracellular matrix: review of its roles in acute and chronic wounds. Published online at World Wide Wounds, URL: http://www.worldwidewounds.com/2005/august/Schultz/Extrace-Matric-Acute-Chronic-Wounds.html.

Sillman, A. L., Quang, D. M., Farboud, B., Fang, K. S., Nuccitelli, R., & Isseroff, R. R. (2003). Human dermal fibroblasts do not exhibit directional migration on collagen 1 in direct-current electric fields of physiological strength. *Exp. Dermatol.*, *12*, 396–402.

Silver, F. H., Freeman, J. W., & DeVore, D. (2001). Viscoelastic properties of human skin and processed dermis. *Skin Res. Technol.*, *7*, 18–23.

Singer, A. J., & Clark, R. A. F. (1999). Cutaneous wound healing. *N. Engl. J. Med.*, *341*, 738–747.

Skalak, R., Zargaryan, S., Jain, R. K., Netti, P. A., & Hoger, A. (1996). Compatibility and the genesis of residual stress by volumetric growth. *J. Math. Biol.*, *34*, 889–914.

Strutz, F., Zeisberg, M., Renziehausin, A., Raschke, B., Becker, V., van Kooten, C., & Muller, G. (2001). TGF-β1 induces proliferation in human renal fibroblasts via induction of basic fibroblast growth factor (FGF-2). *Kidney Int.*, *59*, 579–592.

Thackham, J. A., McElwain, D. L. S., & Long, R. J. (2008). The use of hyperbaric oxygen therapy to treat chronic wounds: a review. *Wound Repair Regen.*, *16*, 321–330.

Thorne, R. G., Hrabetova, S., & Nicholson, C. (2004). Diffusion of epidermal growth factor in rat brain excellular space measured by integrative optical imaging. *J. Neurophysiol.*, *92*, 3471–3481.

Tomasek, J. J., Gabbiani, G., Hinz, B., Chaponnier, C., & Brown, R. A. (2002). Myofibroblasts and mechano-regulation of connective tissue remodelling. *Nat. Rev. Mol. Cell Biol.*, *3*, 349–363.

Tracqui, P., Woodward, D. E., Cruywagen, G. C., Cook, J., & Murray, J. D. (1995). A mechanical model for fibroblast-driven wound healing. *J. Biol. Syst.*, *3*, 1075–1084.

Tranqui, L., & Tracqui, P. (2000). Mechanical signalling and angiogenesis. The integration of cell-extracellular matrix couplings. *Life Sci.*, *323*, 31–47.

Tranquillo, R. T., & Murray, J. D. (1992). Continuum model of fibroblast-driven wound contraction: inflammation-mediation. *J. Theor. Biol.*, *158*, 135–172.

Vande Berg, J. S., Rudolph, R., Poolman, W. L., & Disharoon, D. R. (1989). Comparative growth dynamics and active concentration between cultured human myofibroblasts from granulating wounds and dermal fibroblasts from normal skin. *Lab. Invest.*, *61*, 532–538.

Vermolen, F. J., & Javierre, E. (2010). Computer simulations from a finite-element model for wound contraction and closure. *J. Tissue Viab.*, *19*, 43–53.

Wang, R., Ghahary, A., Shen, Q., Scott, P. G., Roy, K., & Tredget, E. E. (2000). Hypertrophic scar tissues and fibroblasts produce more transforming growth factor-β1 mRNA and protein than normal skin and cells. *Wound Repair Regen.*, *8*, 128–137.

Watts, G. T. (1960). Wound shape and tissue tension in healing. *Br. J. Surg.*, *47*, 555–561.

Waugh, H. V., & Sherratt, J. A. (2006). Macrophage dynamics in diabetic wound healing. *Bull. Math. Biol.*, *68*, 197–207.

Wells, R. G., & Discher, D. E. (2008). Matrix elasticity, cytoskeletal tension, and TGFβ: the insoluble and soluble meet. *Sci. Signal.*, *1*, pe13.

Wipff, P.-J., & Hinz, B. (2008). Integrins and the activation of latent transforming growth factor β1—an intimate relationship. *J. Cell Biol.*, *87*, 601–615.

Wipff, P.-J., & Hinz, B. (2009). Myofibroblasts work best under stress. *J. Bodyw. Mov. Ther.*, *13*, 121–127.

Wipff, P.-J., Rifkin, D. B., Meister, J.-J., & Hinz, B. (2007). Myofibroblast contraction activates latent TGF-β1 from the extracellular matrix. *J. Cell Biol.*, *179*, 1311–1323.

Wrobel, L. K., Fray, T. R., Molloy, J. E., Adams, J. J., Armitage, M. P., & Sparrow, J. C. (2002). Contractility of single human dermal myofibroblasts and fibroblasts. *Cell Motil. Cytoskelet.*, *52*, 82–90.

Xue, C., Friedman, A., & Sen, C. K. (2009). A mathematical model of ischemic cutaneous wounds. *Proc. Natl. Acad. Sci.*, *106*, 16782–16787.

Yang, L., Qiu, C. X., Ludlow, A., Ferguson, M. W. J., & Brunner, G. (1999). Active transforming growth factor-β in wound repair: determination using a new assay. *Am. J. Pathol.*, *154*, 105–111.